Towards an understanding of erosion in ISIS TS-2 spallation neutron targets?

G J Burns, A Dey, D J S Findlay, D J Haynes, D M Jenkins, L G Jones and G P Škoro

Published version information

Citation: G Burns et al. 'Towards an understanding of erosion in ISIS TS-2 spallation neutron targets?' Nuclear Instruments and Methods B, vol. 478 (2020): 158-162.

DOI: 10.1016/j.nimb.2020.06.006

Towards an understanding of erosion in ISIS TS-2 spallation neutron targets?

G J Burns, A Dey, D J S Findlay, D J Haynes, D M Jenkins, L G Jones and G P Škoro
ISIS, Rutherford Appleton Laboratory, Chilton, Oxon., OX11 0QH, UK

Abstract

At the ISIS Spallation Neutron Source at the Rutherford Appleton Laboratory in the UK, lifetimes of tantalum-clad tungsten targets on the Second Target Station (TS-2) have not been as long as expected. Analyses of gamma-ray spectra accumulated in the target services area suggest that erosion within the target is characterised by two exponentially increasing functions of time, one tentatively identified with initial erosion of the tantalum cladding, and the other identified with subsequent leaching of tungsten.

1. Introduction

Spallation neutron sources are particle-accelerator-based user facilities for research into the structure and dynamics of molecular matter using neutrons [1]. At the heart of such sources are high-atomic-number neutron-producing targets driven by high-power proton beams, and the since the targets become highly radioactive in use, long lifetimes of the targets are desirable. Currently, around the world, there are six operational spallation neutron sources of major significance and one under construction: SNS [2] in the USA and J-PARC [3] in Japan use mercury targets, PSI [4] in Switzerland uses a water-cooled zircaloy-clad lead target, LANSCE [5] in the USA originally used a bare water-cooled tungsten target but because of corrosion of the tungsten by the circulating cooling water changed to a water-cooled multi-plate tantalum-clad tungsten target [6], CSNS [7] in China uses a water-cooled multi-plate tantalum-clad tungsten target, and ESS [8] in Sweden is being constructed around a helium-cooled rotating tungsten target. The First Target Station (TS-1) at the ISIS Spallation Neutron Source [9] also uses a water-cooled multi-plate tantalum-clad tungsten target, and over the years much design and operational experience on common target issues has been shared, *e.g.* through the long-running International Collaboration on Advanced Neutron Sources [10] (established in 1977). But in order to maximise the efficiency of cold-neutron production, the Second Target Station (TS-2) [11] at ISIS uses a novel compact tantalum-clad solid tungsten target, and it is operational experience with this new style of target that the present paper reports.

2. The ISIS TS-2 target

The ISIS Spallation Neutron Source is based around an 800-MeV rapidly cycling synchrotron providing protons at 50 pulses per second (pps), each 4–5-μC proton pulse being ~0.5 μs long. Whilst the First Target Station (TS-1) runs at 40 pps, the Second Target Station (TS-2) runs at 10 pps using a target essentially in the form of a solid tantalum-clad tungsten cylinder cooled only at the front end and on the curved surface. The TS-2 target is shown schematically in Fig. 1.

Although TS-2 runs at the relatively modest mean beam power of ~35 kW, since TS-2 began operation in 2008 lifetimes of the TS-2 targets [12] (see Table 1) have been significantly shorter than the ~5-year lifetimes of TS-1 targets, and routine gamma-ray spectrometry has revealed the presence in the TS-2 target cooling water of traces of tungsten in the form of the 24-hour-half-life isotope ^{187}W, showing that tungsten must have been leached out through cracks in the tantalum cladding. The front of TS-2 targets is under stress [13]; the radial profile of the proton beam spot on the target is approximately [14] gaussian with a $1/e$ radius of 0.85 cm, corresponding to a current density on axis of 18 μA cm^{-2}, and for the normal operational proton beam current of ~40 μA at 10 pps the temperature at the nose of the target rises essentially instantaneously by ~20°C ten times a second corresponding to ~10-MPa stress transients [13]. (By contrast, the $1/e$ radius of the proton beam spot on TS-1 targets is 2.5 cm, so that on a 'per pulse' basis TS-2 targets are significantly more highly stressed than TS-1 targets.)

As yet there has not been an opportunity to examine TS-2 targets in detail in a PIE (post-irradiation examination) cave, but an analysis is presented below of gamma-ray spectrometry measurements in order to extract 'remotely' information on corrosion inside the target, particularly as a progressive corrosion mechanism has been proposed [15] whereby increasing quantities of tungsten are leached out into the cooling water as irradiation of the target continues.

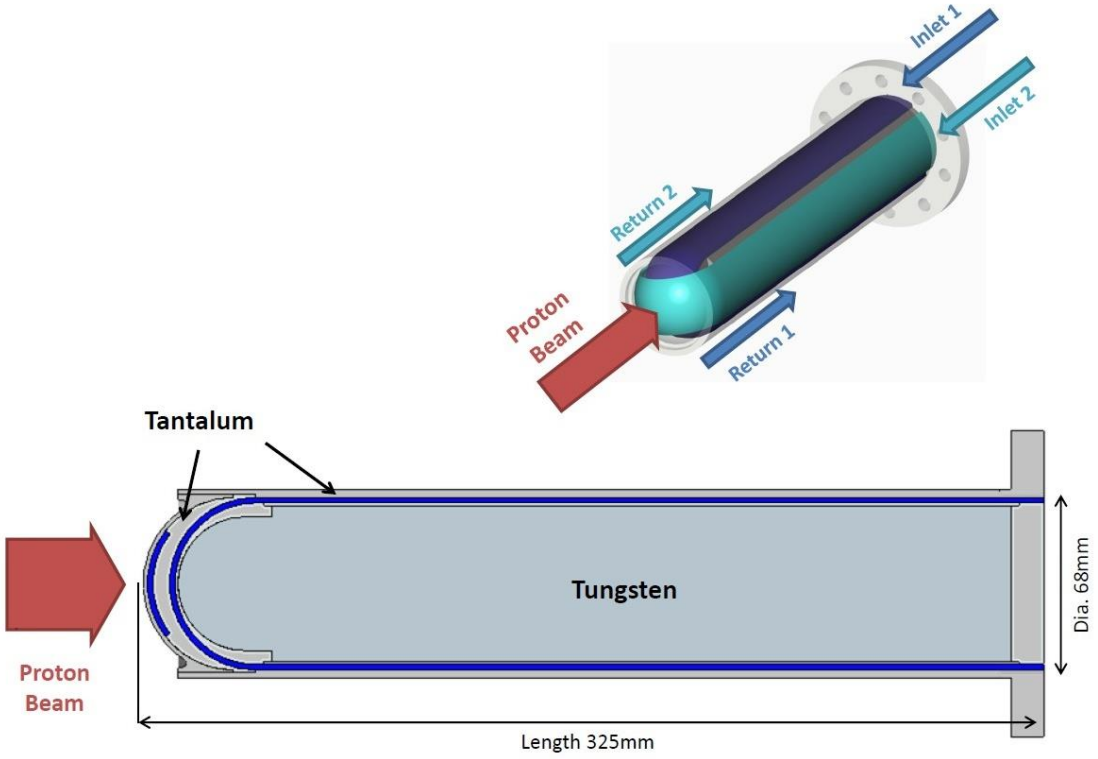

Fig. 1. Schematic drawing of an ISIS TS-2 target. The two water channels cool both the solid cylindrical body and the beam window at the front. Tantalum cladding thickness over tungsten core, 0.9 mm; thickness of tantalum outer casing, 2.3 mm; thickness of water channel between cladding and casing, 2.0 mm. Along axis from front of target: 1.5 mm Ta, 2.0 mm water, 6.0 mm Ta, 2.0 mm water, 1.0 mm Ta. Water (H_2O) circulates through each flow-and-return circuit at a rate of ~45 litres per minute, corresponding to a flow speed of ~10 m s^{-1}.

TS-2 target no.	Irradiated	milliamp-hours
1	Sep. 2008 – Dec. 2009	115
2	Feb. 2010 – May 2010	36
3	Mar. 2011 – Nov. 2012	212
4	Nov. 2012 – Jun. 2014	230
6	Jul. 2014 – Jul. 2015	103
7	Sep. 2015 – Jun. 2017	280
8	Sep. 2017 – Mar. 2019	232
9	Jun. 2019 onwards	

Table 1. Irradiation times of TS-2 targets on ISIS, and integrated proton beam currents delivered to targets during ~30–50-day-long irradiation campaigns ('user runs'). (Target no. 5 was never installed.) Some ~1–2% extra integrated beam current is usually delivered to target before each irradiation campaign for setting up. For target #8, with which the present paper is concerned, the proton fluence on axis was 2.3×10^{21} protons per square centimetre.

3. Measurements and methods

Gamma-ray spectrometry measurements are routinely made in theTS-2 target services area (TSA2) at the ends of ~30–50-day-long irradiation campaigns ('user runs') and during maintenance days within the campaigns, the target services area being where all the plant and equipment is located for circulating and treating the water that cools the target during irradiation — pumps, filters, heat exchangers, ion-exchange columns, *etc*. The gamma-ray spectrometry measurements were carried out using a Canberra Falcon 5000 instrument incorporating a BE2830 HPGe detector [16], and the measured gamma-ray spectra were all accumulated over times of ~3–5 hours beginning 2–3 hours after the proton beam to the target was switched off. The gamma-ray lines counted are listed in Table 2, and Fig. 2 shows the corresponding count rates graphically. The radionuclides listed in Table 2 are radionuclides which appear consistently in the gamma-ray spectra and which are close in mass number to the isotopes of tungsten and tantalum that make up the target, the expectation being that such radionuclides are more likely to provide information that could be used in distinguishing whether the radionuclides were produced from tungsten or tantalum. (Although lines from ^{187}W were readily visible in the gamma-ray spectra, ^{187}W is included in neither Table 2 nor Fig. 2 because its 24-hour half-life is much too short for consistency with the analysis methods presented below.)

The HPGe detector was always placed at the same position within the target services area, and although in operation the target cooling water is continuously passed through filters and ion-exchange resin beds, no residues trapped in the filters or in the ion-exchange resin beds were removed during the period of time spanned by the present measurements. Consequently, the gamma-ray-line count rates at the fixed location in the target services area have been assumed to be proportional to the activities of the radionuclides in the material eroded from the target.

Radionuclide	Half-life (days)	Gamma-ray line (keV)	Emission probability (%)
^{171}Lu	8.2	740	47.9
^{172}Lu	6.7	1094	62.5
^{172}Hf	683	126	11.3
^{175}Hf	70	343	84.0
^{182}Ta	114	1121	35.2
^{183}Re	71	292	3.05
^{184}Re	38	792	37.7
^{184m}Re	169	920	8.22

Table 2. The eight radionuclides and count rate signatures analysed in the present work. For each radionuclide the gamma-ray line counted was the most easily visible in the spectrum, not necessarily the line with the greatest emission probability.

4. Phenomenological model

For the present purpose, it will be assumed that apart from activity induced in the cooling water itself, activity in the target services area arises from radionuclides leached by the cooling water out of the radioactive target. It will also be assumed that the number of atoms N of a radionuclide is given by integration of the differential equation $dN = r(t)\, i(t)\, dt - \lambda\, N\, dt$, *i.e.* in an infinitesimally small time interval dt, $r(t)\, i(t)\, dt$ atoms are produced where $r(t)$ is a production rate per unit beam current and per unit time and is a function of time t, $i(t)$ is the beam current and is a function of t, and $\lambda\, N\, dt$ atoms decay where $\lambda = \ln(2)/t_{1/2}$ is the decay constant and $t_{1/2}$ is the half-life. The intention is to parametrise $r = r(t)$ in some plausible way and fit the resultant solution of the differential equation to measured count rate data in order to extract the parameters of $r = r(t)$. Of course, the count rate C of a gamma-ray line measured by a gamma-ray detector in the target services area is not the number of atoms N of the corresponding radionuclide, but C is related to N through $C = \alpha\, \eta\, \varepsilon\, \lambda N$ where α is the emission probability of the gamma-ray line being measured, η represents absorption of gamma-rays in material lying between the source of gamma-rays and the detector, ε is the absolute detection efficiency of the detector, and λN is the activity of the N atoms (so that $\alpha\, \eta\, \varepsilon\, \lambda$ represents count rate per atom). By writing $N = C/(\alpha\, \eta\, \varepsilon\, \lambda)$ and substituting, the differential equation above may be re-written as

$$dC = r'(t)\, i(t)\, dt - \lambda\, C\, dt \qquad (1)$$

where $r'(t) = \alpha\, \eta\, \varepsilon\, \lambda\, r(t)$ is simply the production rate re-cast in terms of count rate.

If a parent nucleus or an isomer state (hereinafter both denoted by *p*) can contribute to an observed count rate (*e.g.* as 1.87-year ^{172}Hf is the parent of 6.7-day ^{172}Lu, and as the 169-day isomer ^{184m}Re can decay to the 38-day ground state of ^{184}Re) then the equations become $dN_g = r_g(t)\, i(t)\, dt + f_{pg}\, \lambda_p\, N_p\, dt - \lambda_g\, N_g\, dt$ for the ground state and $dN_p = g_{pg}\, r_g(t)\, i(t)\, dt - \lambda_p\, N_p\, dt$ for the parent or isomer where g denotes ground state, p denotes parent or isomer, f_{pg} is the fraction of the parent or isomer that decays to the daughter or ground state, and g_{pg} is the ratio of the production rate to the parent or isomer to the production rate directly to the daughter or ground state. Re-

casting in terms of count rates $C_g = \alpha_g\, \eta_g\, \varepsilon_g\, \lambda_g N_g$ and $C_p = \alpha_p\, \eta_p\, \varepsilon_p\, \lambda_p N_p$ leads to

$$dC_g = r'_g(t)\, i(t)\, dt\, +\, f_{pg}\, R_{gp}\, \lambda_p\, C_p\, dt\, -\lambda_g\, C_g\, dt \qquad (2)$$

and to

$$dC_p = (g_{pg}/R_{gp})\, r'_g(t)\, i(t)\, dt\, -\lambda_p\, C_p\, dt \qquad (3)$$

where $R_{gp} = (\alpha_g\, \eta_g\, \varepsilon_g\, \lambda_g)/(\alpha_p\, \eta_p\, \varepsilon_p\, \lambda_p)$.

5. Analysis

As already stated above, the overall intention is to extract a production rate per unit beam current and per unit time $r(t)$ as a function of time t for each radionuclide. Following the suggestion already referred to in Sect. 1 that the rate of erosion or leaching of target material starts slowly but increases with time t, the form $r'(t) = a_0 + a_1 \exp(a_2\, t)$ was chosen.

For radionuclides the production of which is not complicated by the involvement of parents or isomers, the equation $dC = r'(t)\, i(t)\, dt - \lambda\, C\, dt$ (Eq. 1 above) was integrated in 1-day steps, and a 4-parameter fit [17] was made to the count rate data, the four parameters being a_0, a_1, a_2 (from the production rate $r'(t)$) and $C_{t=0}$ (the count rate at time zero when the integration began).

For radionuclides contributions to the production of which can come from parents or isomers, the two equations $dC_g = r'_g(t)\, i(t)\, dt\, +\, f_{pg}\, R_{gp}\, \lambda_p\, C_p\, dt\, -\lambda_g\, C_g\, dt$ and $dC_p = (g_{pg}/R_{gp})\, r'_g(t)\, i(t)\, dt\, -\lambda_p\, C_p\, dt$ (Eqs. 2 and 3 above) were integrated in 1-day steps and fitted simultaneously to the count rate data for the daughter and parent or for the ground state and isomer. In such cases a 7-parameter fit was made, the seven parameters being a_0, a_1 and a_2, two count rates at time zero, and g_{pg} and R_{gp}. The quantity f_{pg}, the fraction of the parent or isomer that decays to the daughter or ground state, is a known quantity, unity for ^{172}Hf $\rightarrow$ ^{172}Lu, and 0.754 for ^{184m}Re $\rightarrow$ ^{184}Re [18].

The resultant fits to the count rate data are shown in Fig. 2, and the production rate functions $r'(t)$ extracted from the fits are shown in Fig. 3. It should be noted that the vertical scale in Fig. 3 is logarithmic, so that the 'straight lines' that appear therein are actually describing production rates that are increasing exponentially with time, and at later times the two noticeably-upward-bending curves are increasing with time even more rapidly.

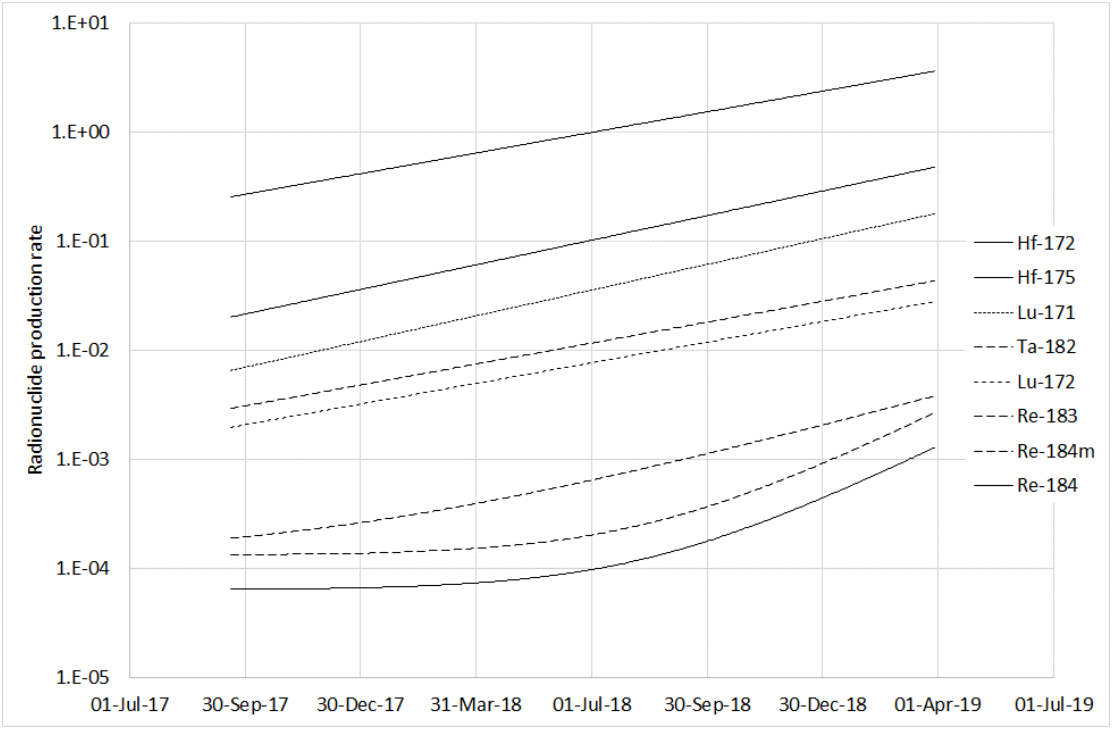

Fig. 3. Radionuclide production rates $r'(t)$ (counts per second per day per microamp of proton beam) extracted by fitting the count rate data. Note that only the shapes of the production-rate curves are relevant, since corrections have been made for neither gamma-ray emission probability nor absorption nor gamma-ray detection efficiency. Also note that since the vertical scale is logarithmic, 'straight lines' actually denote exponential increases. The vertical order of the curves is the same as the vertical order of the labels. (Because of differences in half-lives, the vertical order of radionuclides in this figure is not the same as the vertical order of radionuclides in Fig. 2.)

6. Discussion

In Fig. 2 it is clear that whilst the fits may reproduce the principal features of the data, they do not reproduce all the detail. But it may be unrealistic to expect very good fits; the measured activity in the target services area is either activity circulating in the water or activity deposited in filters, ion-exchange resin beds, insides of pipes, pumps, heat exchangers, *etc.*, and it is perfectly possible that over time the activity can move from place to place so that both absorption in material lying between the activity and the gamma-ray detector, and the distance between the activity and the gamma-ray detector, change with time; consequently count rate may not always be proportional to activity.

The least good fit in Fig. 2 is the fit to ^{171}Lu. This is perhaps because ^{171}Lu is the radionuclide that effectively has the shortest half-life (although the half-life of ^{172}Lu on its own is slightly shorter than the half-life of ^{171}Lu, the effective half-life of ^{172}Lu in the present context is much longer since most of the ^{172}Lu activity actually comes from its long-lived parent ^{172}Hf), and the inevitable day-to-day variations in beam current delivered to the target and ignored in the present model may therefore have the greatest effect on ^{171}Lu activity. (The same day-to-day variations would have effectively precluded any attempts to fit to ^{187}W count rates, since the half-life ^{187}W is much shorter than the half-life of ^{171}Lu.)

The one obvious feature of Fig. 3 is that whilst the production rates of five of the radionuclides appear as straight lines as plotted, the production rate of ^{183}Re curves slightly upwards, and the production rates of ^{184}Re and ^{184m}Re curve noticeably upwards. A comparison is presented in Table 3, wherein values are given of the a_2 parameter in the parametrisation of the production rate, a_2 being the asymptotic slope on a logarithmic scale, and the same comparison is given graphically in Fig. 4. It is clear that the behaviour of the five radionuclides ^{171}Lu – ^{182}Ta is different from the behaviour of the rhenium radionuclides. Since the rhenium radionuclides can come only[1] from tungsten, whereas all the other radionuclides can also come from tantalum, a plausible interpretation may be that initially activity in the cooling water appears as spallation and neutron-capture products eroded from the tantalum cladding over which the cooling water is flowing rapidly, and only after some time does tungsten start to gradually appear in the water, but after the tungsten does start to appear, leaching of tungsten increases rapidly. Such an interpretation is not inconsistent with the suggestion referred to in Sect. 1, *viz* that initially the integrity of the tantalum cladding is complete, but after some time a crack in the cladding allows the cooling water to reach tungsten, and then the crack opens up, slowly at first, but increasingly quickly as time goes on.

Experience with targets at other spallation neutron sources is not immediately relevant to the present TS-2 target issues. SNS, J-PARC and PSI run completely different target systems; LANSCE's multi-plate tantalum-clad tungsten target appears to be running satisfactorily; CSNS has not been running long enough for significant operational experience to be accumulated; ESS is still under construction; and no sign of tungsten in the cooling water for TS-1 targets at ISIS has ever been observed. Consequently, over the past few years an R&D programme aimed at extending lifetimes of TS-2 targets has been in place [12], and much work has already been carried out in investigating and improving areas of potential weakness in the tantalum cladding such as lack of sufficient weld penetration when joining two sections of cladding, grain growth during electron-beam welding, and loss of material when assemblies joined by hot isostatic pressing (HIP) are machined, but all such work has been carried out before targets or parts thereof were irradiated. Obviously, it would be of great interest to examine targets physically after irradiation to establish where the weaknesses actually were, and to see whether the present evidence gathered through gamma-ray spectrometry can be confirmed. However, such an examination would involve cutting into highly radioactive material, and at present the resources necessary in terms of PIE caves are not available, although plans for a 'hot cell' at ISIS that could be used for the purpose are currently being pursued.

[1] The mass number (183) of the lighter of the two rhenium radionuclides is greater by 2 than the mass number (181) of the higher-mass isotope in naturally occurring tantalum.

7. Summary and conclusions

Gamma-ray spectrometry data recorded in the target services area of the Second Target Station (TS-2) on the ISIS Spallation Neutron Source throughout the period of time that tantalum-clad tungsten target W#8 was installed and operating have been analysed to extract radionuclide production rates of as a function of time, thereby demonstrating a method of assessing corrosion remotely when physical examination is not practicable. The production rates are characterised by exponentially increasing functions of time, and they fall into two categories, tentatively identified with initial erosion of the tantalum cladding and subsequent leaching of tungsten. Such an interpretation is consistent with a suggested progressive corrosion mechanism whereby increasing quantities of tungsten are leached out into the cooling water as irradiation of the target continues.

References

[1] G S Bauer, Nucl. Instr. Meth. A463 (2001) 505.

[2] https://neutrons.ornl.gov/sns

[3] https://j-parc.jp/c/en/index.html

[4] https://www.psi.ch/en/sinq

[5] https://lansce.lanl.gov/

[6] A T Nelson *et al.*, J. Nucl. Mater. 431 (2012) 172.

[7] http://english.ihep.cas.cn/csns/doc/1959.html

[8] https://europeanspallationsource.se/

[9] https://www.isis.stfc.ac.uk/

[10] For example, ICANS XXIII, https://conference.sns.gov/event/138/timetable/?view=standard

[11] J W G Thomason, Nucl. Instr. Meth. A917 (2019) 61.

[12] A Dey and L G Jones, J. Nucl. Mater. 506 (2018) 63.

[13] http://pasi.org.uk/images_pasi/a/a0/05-Wilcox-28Feb13.pdf

[14] D J S Findlay, B Jones and D J Adams, Nucl. Inst. Meth. A889 (2018) 113.

[15] A Dey, private communication.

[16] L J Harkness-Brennan *et al.*, Nucl. Instr. Meth. A760 (2014) 28.

[17] Minimisation routine VA04A, Harwell Subroutine Library, https://www.hsl.rl.ac.uk/

[18] 'Table of Isotopes', ed. R B Firestone and V S Shirley, Wiley InterScience, 1996.

Radionuclide	a_2, per day		
^{171}Lu	0.00594	±	0.00205
^{172}Lu	0.00480	±	0.00071
^{172}Hf	0.00480	±	0.00071
^{175}Hf	0.00568	±	0.00110
^{182}Ta	0.00484	±	0.00062
^{183}Re	0.00720	±	0.00239
^{184}Re	0.01320	±	0.00565
^{184m}Re	0.01320	±	0.00565

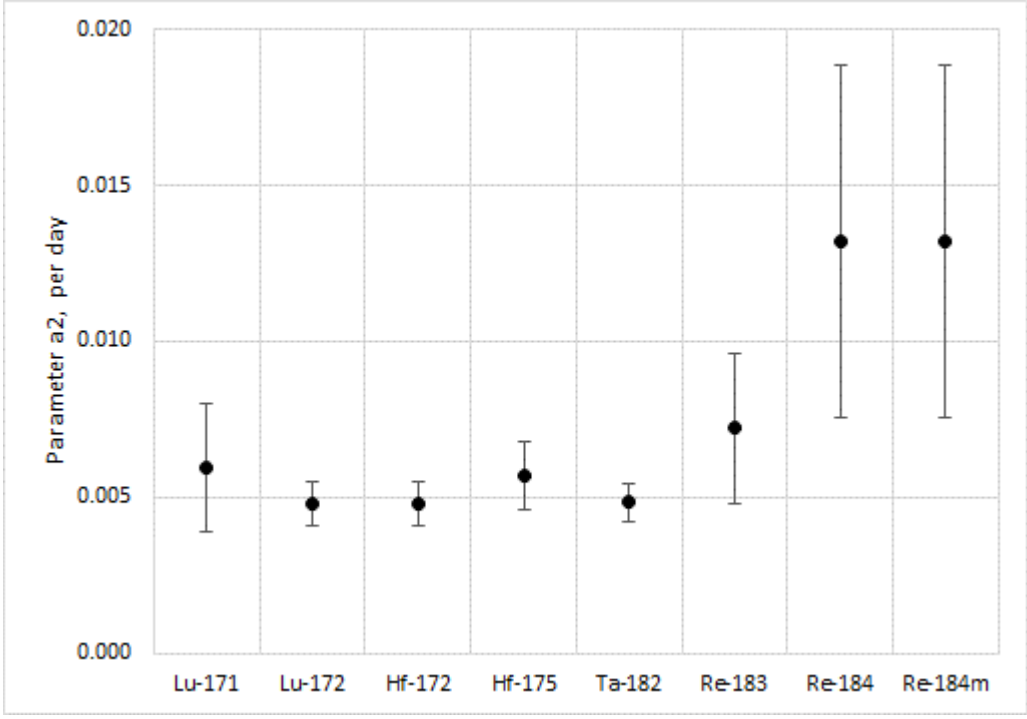

Table 3 and Fig. 4. Values of the a_2 parameter in the parametrisation of the production rate $r'(t) = a_0 + a_1 \exp(a_2\, t)$, a_2 representing the asymptotic slopes in Fig. 3. The uncertainties were established by repeatedly (≥300 times) perturbing the count rates C by amounts randomly chosen from gaussian distributions with standard deviations δC and refitting, and then taking standard deviations of the sets of 'perturbed' a_2 values.

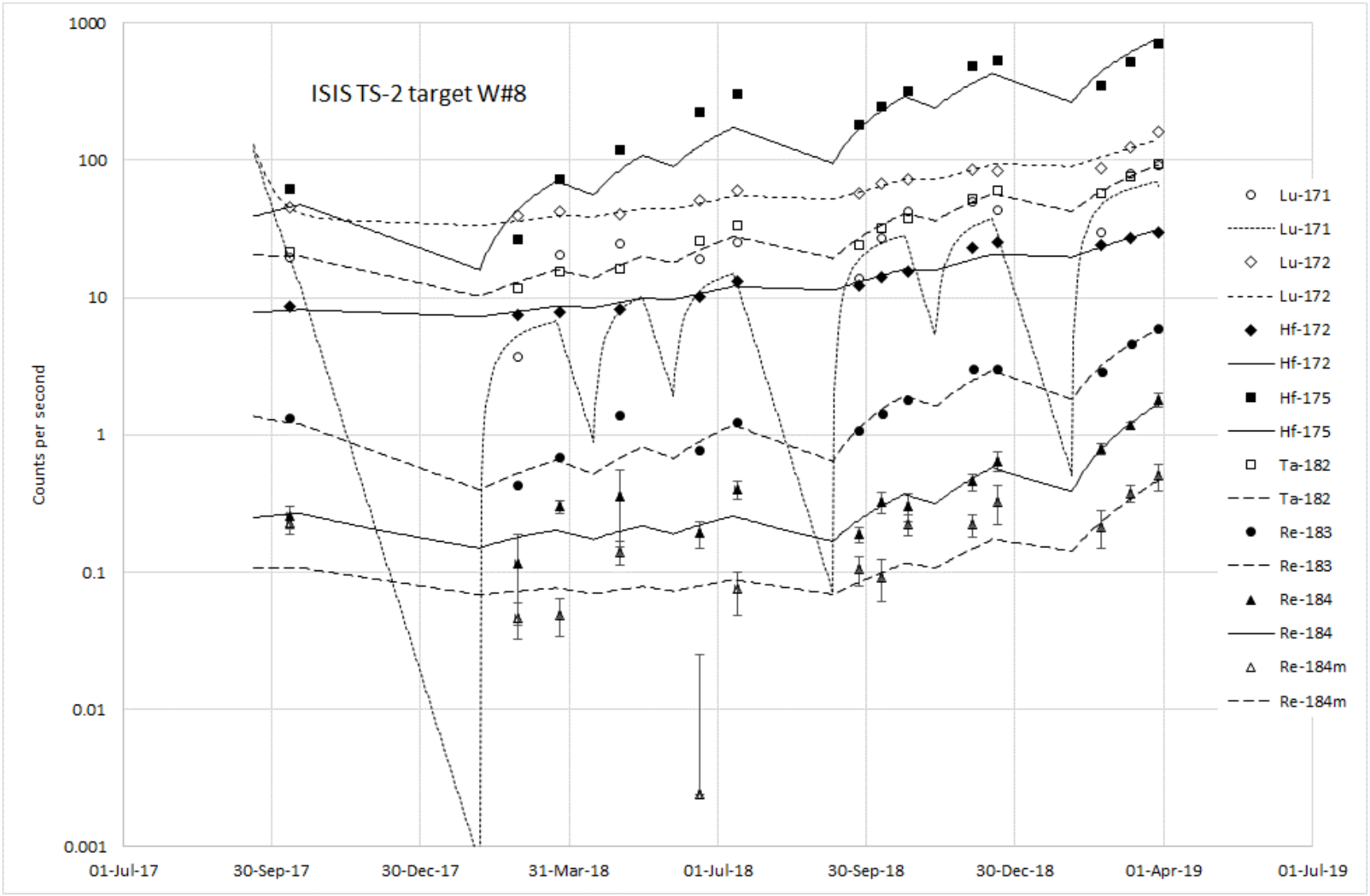

Fig. 2. Gamma-ray count rates (data points, with uncertainties shown explicitly when greater than ±10%) for eight radionuclides measured by gamma-ray spectrometry in the target services area of the ISIS Second Target Station, and fits to the count rate data as described in Sect. 4.